ACS EARTH AND SPACE CHEMISTRY

Article

Cite This: ACS Earth Space Chem. 2019, 3, 718−727

http://pubs.acs.org/journal/aesccq

Photochemical Formation Process of Schwertmannite on Montmorillonite and Corresponding Cr(VI) Adsorption Capacity

Zhipeng Shu,[†] Lihu Liu,[†] Guohong Qiu,*[,†] Xiong Yang,[†] Mingzhe Zhang,[†] Wenfeng Tan,[†] Chengshuai Liu,[‡] and Fei Wu[‡]

[†]Key Laboratory of Arable Land Conservation (Middle and Lower Reaches of Yangtze River), Ministry of Agriculture and Rural Affairs, Hubei Key Laboratory of Soil Environment and Pollution Remediation, College of Resources and Environment, Huazhong Agricultural University, Wuhan 430070, Hubei Province, China

[‡]State Key Laboratory of Environmental Geochemistry, Institute of Geochemistry, Chinese Academy of Sciences, Guiyang 550081, China

Supporting Information

ABSTRACT: The formation and transformation of schwertmannite affect the migration, conversion, and toxicity of chromium (Cr) in soils and sediments. Schwertmannite could be obtained from the oxidation of Fe(II) by hydroxyl radicals ($OH^{\bullet}$) and superoxide radicals ($O_2^{\bullet-}$) generated from the photolysis of NO_3^- under acidic and sulfate-rich conditions. As one of the most abundant components, montmorillonite is widely distributed in soils and sediments. However, the effect of montmorillonite on the photochemical formation process and corresponding Cr adsorption behaviors of schwertmannite remains elusive. This study indicates that schwertmannite could be formed on the montmorillonite surface during the photocatalytic oxidation of dissolved Fe(II). The formation rate, particle size, and crystallinity degree of schwertmannite formed on montmorillonite surface increased with increasing $FeSO_4$ concentration (1.0−5.0 mmol L^{-1}). The presence of montmorillonite led to a decrease in the particle size of schwertmannite. When the initial concentration of Fe(II) was 5.0 mmol L^{-1}, the specific surface area of schwertmannite−montmorillonite aggregates reached 243.3 m^2 g^{-1}, which was remarkably larger than that of single-phase schwertmannite (24.6 m^2 g^{-1}) and montmorillonite (138.1 m^2 g^{-1}). The schwertmannite−montmorillonite aggregates showed a higher adsorption capacity for Cr(VI) (97.4 mg Cr g^{-1} Fe) than single-phase schwertmannite (72.9 mg Cr g^{-1} Fe). This work reveals the possible formation pathway and Cr adsorption behavior of schwertmannite on the surface of montmorillonite in waters and soils.

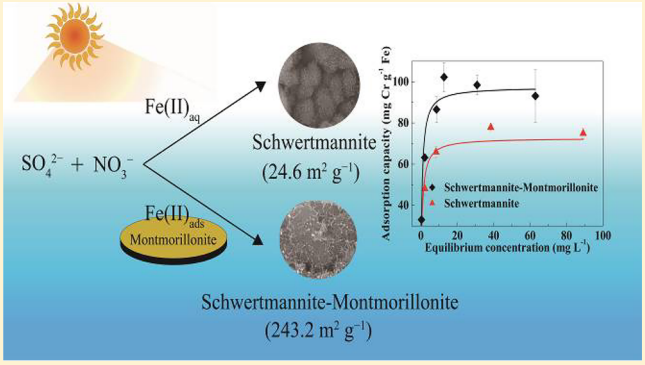

KEYWORDS: *Solar irradiation, NO_3^-, Schwertmannite, Montmorillonite, Adsorption, Cr(VI)*

1. INTRODUCTION

As a nanocrystalline ferric oxyhydroxy-sulfate mineral, schwertmannite ($Fe_8O_8(OH)_{8-2x}(SO_4)_x \cdot nH_2O$, $1 \leq x \leq 1.75$) is widely distributed in acidic and sulfate-rich environments including tailing, sediments of mine-pit lakes, and acid-sulfate soils.[1] The double chains of edge-sharing FeO_6 octahedra in schwertmannite form 2 × 2 tunnels. The sulfate ions (SO_4^{2-}) in the tunnels can stabilize the structure of schwertmannite.[2] Compared with ferrihydrite, goethite, and hematite, schwertmannite may inhibit the mobility and bioavailability of anions and cations by coprecipitation or adsorption due to its larger specific surface area and high adsorption activity.[3−5]

Chromium (Cr) contamination arising from leather tanning, paint making, and landfill has been commonly found in soils and groundwater environments.[3,4] In general, Cr(III) and Cr(VI) are stable and predominant forms in natural environments. Due to its higher solubility and mobility, Cr(VI) is more harmful to plants, animals, and humans than Cr(III) and exists mainly in the forms of oxyanions chromate (CrO_4^-) and dichromate ($Cr_2O_7^{2-}$).[4] SO_4^{2-} in schwertmannite structure can be substituted by oxyanions (CrO_4^{2-}, AsO_3^{3-}, and AsO_4^{3-}) for their similar structures.[5,6] These oxyanions can participate in the formation of schwertmannite as chemical components and also affect the stability and reactivity of schwertmannite.[2,3,5−7]

Schwertmannite is commonly formed through the oxidation of Fe(II) by O_2, microorganisms, and reactive oxygen species (ROS) and the hydrolysis of $Fe(III)_{aq}$ in acidic and sulfate-rich aqueous environments.[7−9] Different formation pathways will

Special Issue: Iron Redox Chemistry and Its Environmental Impact

Received: December 13, 2018
Revised: March 23, 2019
Accepted: March 27, 2019
Published: March 27, 2019

DOI: 10.1021/acsearthspacechem.8b00202
ACS Earth Space Chem. 2019, 3, 718−727

result in different particle size, specific surface area, and micromorphology of schwertmannite, which will affect its adsorption behavior for Cr(VI). During the formation process of schwertmannite, the rapid oxidation of Fe(II) leads to increased hydrolysis and precipitation rate of Fe(III), which enhances the nucleation rate and inhibits the crystal growth rate, resulting in decreases in the particle size of schwertmannite to form colloidal size agglomerate.[10] The aggregation of schwertmannite decreases the effective surface area of schwertmannite, resulting in reduced absorption capacity for Cr(VI).[7,8,10] For example, the specific surface area and maximum Cr(VI) adsorption capacity of the schwertmannite generated from the slow hydrolysis of Fe(III) could reach 165 $m^2\ g^{-1}$ and 178 mg g^{-1}, respectively, while those of the schwertmannite formed from the oxidation of Fe(II) by *Acidithiobacillus ferrooxidans* are respectively 5−14 and 55 mg g^{-1}.[11,12] $O_2^{\bullet-}$ and $OH^{\bullet}$ generated from the photolysis of NO_3^- under solar irradiation can also readily oxidize Fe(II) to schwertmannite in acidic and sulfate-rich environments.[13] Compared with traditional preparation pathways in laboratory, photochemical formation can better represent the possible formation process of schwertmannite in natural environments. However, the formation and corresponding adsorption behavior of heavy metal ions by schwertmannite formed through photochemical pathway still remain elusive.

In natural environments, some impurities including organic matter, silicon, and clay minerals often coexist with Fe(II) or Fe(III) during the formation of schwertmannite. These impurities would affect the surface activity and heavy metal ion absorption capacity of schwertmannite.[14] As common substances in soils and sediments, clay minerals can significantly inhibit the formation and transformation of low crystallinity Fe(III) oxides including schwertmannite, ferrihydrite, and jarosite by retarding the crystallization process of Fe(III).[15−18] Therefore, clay minerals could affect the formation process and physicochemical properties of schwertmannite, including morphology, particle size, surface charge, and adsorption capacity.

Montmorillonite is composed of tetrahedral SiO_4 and octahedral AlO_6 sheets with a typical 2:1 phyllosilicate structure.[19,20] The substitution of Si^{4+} in tetrahedra by Al^{3+} and Al^{3+} in octahedra by Mg^{2+} results in the net negative surface charge of montmorillonite, which facilitates the adsorption for $Fe(II)_{aq}$.[19,20] As one of the most abundant redox active species in anaerobic soils and sediments, Fe(II) affects the fate of contaminants through the formation of iron oxides.[21,22] The oxidation of Fe(II) on montmorillonite surface may lead to the formation of schwertmannite−montmorillonite aggregate due to the electrostatic force between montmorillonite and Fe(II) in acidic and sulfate-rich environments.[23−26] Therefore, the effects of montmorillonite on the crystallinity degree, micromorphology, and Cr(VI) adsorption capacity of photochemically synthesized schwertmannite remain largely unknown and need further investigations.

In this work, the photochemical formation process of schwertmannite on montmorillonite surface was investigated, and the effects of $Fe(II)_{aq}$ and SO_4^{2-} concentrations on the micromorphology, particle size, and the corresponding Cr(VI) adsorption capacity of schwertmannite were also studied. The results are expected to expand our understanding of the possible formation pathway of schwertmannite in supergene environments and its adsorption behavior for Cr(VI).

2. EXPERIMENTAL SECTION

2.1. Photochemical Formation of Schwertmannite. Schwertmannite was synthesized through the photochemical method as previously reported.[13] About 100 mL of mixed solution of $NaNO_3$ (100 mmol L^{-1}) and $FeSO_4$ (1.0, 3.0, and 5.0 mmol L^{-1}) was prepared in a 150 mL quartz tube in an anaerobic glovebox. The pH of the mixed solution was adjusted to 6.0 (± 0.05) with NaOH (1.0 mmol L^{-1}). The final dissolved oxygen in the suspension was measured to be 0.3 ppm using a dissolved oxygen meter (JPB-607A). The sealed quartz tubes were taken out from the anaerobic glovebox and then put into a PL-03 photochemical reactor equipped with a 1000 W mercury lamp (Beijing Precise Technology Co., Ltd.) for 8 h. The light intensity at 320−400 nm was determined to be 5.0 mW cm^{-2} by the UV-A irradiatometer (Photoelectric Instrument Factory of Beijing Normal University), and the light with $\lambda > 420$ nm was removed by light filter. The final products were collected by filtration through 0.22 μm nitrocellulose membranes, dried at 40 °C overnight in DZF−6021 vacuum drying oven (Yiheng Instrument Factory Co. Ltd., China), and stored in anaerobic glovebox. The products were designated as Sch-1, Sch-3, and Sch-5 when the concentrations of $FeSO_4$ were 1.0, 3.0, and 5.0 mmol L^{-1}, respectively.

In order to investigate the influence of montmorillonite on the photochemical formation process of schwertmannite, 0.1 g L^{-1} montmorillonite (Aladdin Shanghai Co., Ltd.) was added to the mixed solution of $NaNO_3$ (100 mmol L^{-1}) and $FeSO_4$ (1.0, 3.0, and 5.0 mmol L^{-1}) with pH 6.0 under UV light for 8 h in nitrogen atmosphere. The pH decreased from 6.0 to 2.73, 2.42, and 2.50 when the concentrations of $FeSO_4$ in the reaction system were 1.0, 3.0, and 5.0 mmol L^{-1}, respectively. The samples were designated as Sch-1Mt, Sch-3Mt, and Sch-5Mt in the presence of montmorillonite when the concentrations of $FeSO_4$ were controlled at 1.0, 3.0, and 5.0 mmol L^{-1}, respectively. To investigate the effect of SO_4^{2-} concentration on the micromorphology of schwertmannite, a certain amount of Na_2SO_4 was added to the mixed solution of $NaNO_3$ (100 mmol L^{-1}) and $FeSO_4$ (1.0 and 3.0 mmol L^{-1}). The initial concentration of SO_4^{2-} in the reaction system was 5.0 mmol L^{-1}. The samples were designated as Sch-1Mt-4S and Sch-3Mt-2S when the addition of Na_2SO_4 was controlled to be 4.0 and 2.0 mmol L^{-1}, respectively. In order to simplify the description, the names of products and experimental conditions were summarized as Table 1.

2.2. Batch Adsorption Experiments. The Cr(VI) isothermal adsorption experiments were operated at pH 6.0

Table 1. Reaction Conditions and Product Names

product names	reaction conditions[a]
Sch-1	100 mmol L^{-1} $NaNO_3$, 1.0 mmol L^{-1} $FeSO_4$
Sch-3	100 mmol L^{-1} $NaNO_3$, 3.0 mmol L^{-1} $FeSO_4$
Sch-5	100 mmol L^{-1} $NaNO_3$, 5.0 mmol L^{-1} $FeSO_4$
Sch-1Mt	100 mmol L^{-1} $NaNO_3$, 1.0 mmol L^{-1} $FeSO_4$, 0.1 g L^{-1} Mt
Sch-3Mt	100 mmol L^{-1} $NaNO_3$, 3.0 mmol L^{-1} $FeSO_4$, 0.1 g L^{-1} Mt
Sch-5Mt	100 mmol L^{-1} $NaNO_3$, 5.0 mmol L^{-1} $FeSO_4$, 0.1 g L^{-1} Mt
Sch-1Mt-4S	100 mmol L^{-1} $NaNO_3$, 1.0 mmol L^{-1} $FeSO_4$, 0.1 g L^{-1} Mt, 4.0 mmol L^{-1} Na_2SO_4
Sch-3Mt-2S	100 mmol L^{-1} $NaNO_3$, 3.0 mmol L^{-1} $FeSO_4$, 0.1 g L^{-1} Mt, 2.0 mmol L^{-1} Na_2SO_4

[a]All reactions were under UV, pH 6.0, 8 h.

DOI: 10.1021/acsearthspacechem.8b00202
ACS Earth Space Chem. 2019, 3, 718−727

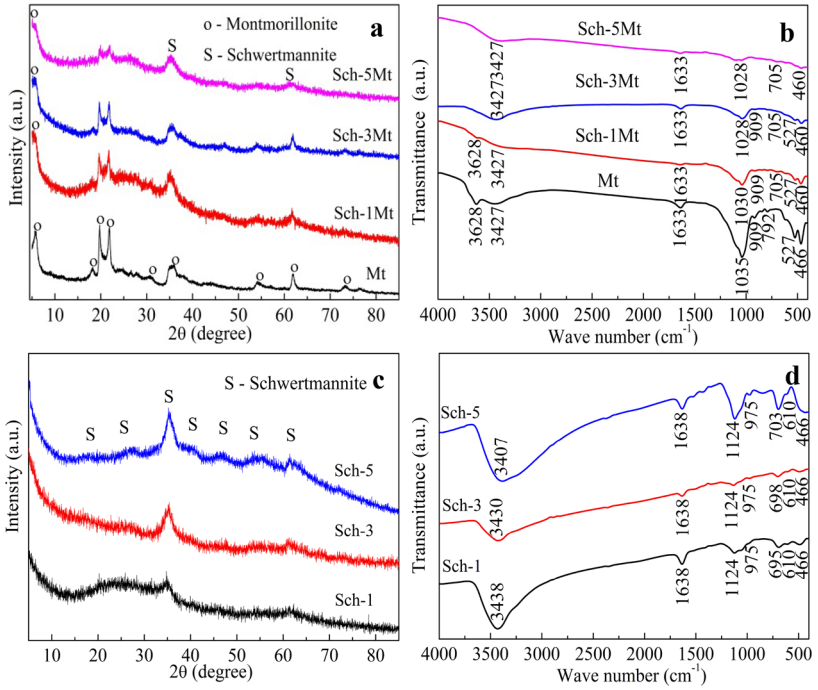

Figure 1. XRD patterns and FTIR spectra of montmorillonite (Mt) and as-obtained schwertmannite−montmorillonite aggregates (Sch-1Mt, Sch-3Mt, and Sch-5Mt) (a,b) and single-phase schwertmannite (Sch-1, Sch-3, and Sch-5) (c,d).

and 25 °C in 0.1 mol L^{-1} $NaNO_3$ solution. First, 0.75 g of samples (Sch-1, Sch-3, Sch-5, Sch-1Mt, Sch-3Mt, Sch-5Mt, and montmorillonite) were dispersed in 0.1 mol L^{-1} $NaNO_3$ solution of 250 mL. Then, 10 mL of suspension and 0.25−10 mL of $K_2Cr_2O_7$ solution (400 mg L^{-1}) were added to a 50 mL centrifuge tube. During the isothermal adsorption, the total volume of the solution was controlled at 20 mL using $NaNO_3$ (0.1 mol L^{-1}), and the concentration of samples was 1.5 g L^{-1}. All the adsorption experiments were conducted in triplicate at room temperature (25 ± 1 °C) and shaken at 250 r min^{-1} for 24 h. After 24 h of reaction, 5 mL of supernatant was immediately filtered through 0.22 μm membrane filter to determine the Cr(VI) concentration of the solution. To investigate the influence of pH on the Cr(VI) adsorption on schwertmannite, the Cr(VI) adsorption experiments on Sch-5Mt were conducted with different pH values (3.0 and 4.5) at 25 °C for 24 h. In order to identify the mechanism of Cr(VI) removal, Cr(VI) desorption from Sch-5Mt (1.5 g L^{-1}) was conducted at pH 6.0. The solid product after isothermal adsorption for 24 h was treated with K_2HPO_4 (0.1 mol L^{-1}) for 3 h. The supernatant was collected and separated through a membrane filter to determine the Cr(VI) and total Cr concentration in the solution. The concentration of NO_3^- in solutions was determined by ion chromatography (Dionex ICS-1100).

2.3. Characterization and Analysis. The final products were characterized by X-ray diffractometer (XRD, Bruker D8 Advance diffractometer with Cu Kα, λ = 0.15418 nm). The XRD patterns were collected at a step size of 0.02 using a scanning rate of 2° min^{-1} with the range of 2-theta from 5° to 85°. The XRD peaks were identified by EVA software. The characteristic functional groups of the solid products were characterized by Fourier-transform infrared spectroscopy (FTIR, Bruker VERTEX 70). The morphology and particle size of the samples were examined through field emission scanning electron microscopy (FESEM, HITACHI, SU8000) and transmission electron microscopy (TEM, FEI, Talos F200C). Sample collection for TEM was performed in an anoxic glovebox. The mixed solution of montmorillonite (0.1 g L^{-1}), $NaNO_3$ (100 mmol L^{-1}), and $FeSO_4$ (5.0 mmol L^{-1}) was exposed to UV light irradiation for 8 h in nitrogen atmosphere at initial pH 6.0. The wet solid products were immediately collected by using a 0.22 μm membrane filter and transferred to a 50 mL centrifuge tube. Then, about 5 mL of ethanol was added to the centrifuge tube to disperse the solid product from the membrane. The centrifuge tube was shaken slightly without ultrasound to form a suspension for further TEM characterization. Mössbauer spectra were collected at 12 K in transmission mode and a WSS-10 Mössbauer spectrometer (WissEL GmbH, Germany) equipped with a closed cycle cryostat (SHI-850, Janis Research Co., Wilmington, MA, USA). All spectra were calibrated against 7 μm α-Fe(0) foil and fit using Mosswinn software. Specific surface area of the samples was measured using Micromeritics ASAP 2020.

Microwave digestion instrument (CEM, MARS 6, USA) was used to determine the Fe content of the samples. First, 50 mg of sample was precisely weighed and transferred to a microwave digestion vessel. Then, 6 mL of HCl, 2 mL of HNO_3, and 2 mL of HF were added to the vessels, which were placed in the digestion instrument and heated for 40 min at 190 °C. The concentrations of Cr(VI) were determined by UV−visible spectrophotometer (UV-1800, Shanghai Mapada Instruments Co., Ltd., China), and the concentrations of Fe(II) were spectrophotometrically determined at 510 nm using 1,10-phenanthroline as color developer.[27,28] The zeta potential values of samples were determined in $NaNO_3$ (1.0 mmol L^{-1}) using a Zetasizer 3600 (Malvern Instrument, USA). The pH values of the suspension (0.1 g L^{-1}) were, respectively, adjusted to 2.0−10.0 by NaOH (0.1 and 0.5 mol L^{-1}) and HNO_3 (0.1 and 0.5 mol L^{-1}).

DOI: 10.1021/acsearthspacechem.8b00202
ACS Earth Space Chem. 2019, 3, 718−727

To detect the presence of reactive oxygen species (ROS) in the reaction systems, methanol (MeOH, 100 mmol L^{-1}), and nitro blue tetrazolium (NBT, 100 mg L^{-1}) were used to qualitatively determine $OH^{\bullet}$ and $O_2^{\bullet-}$, respectively. Benzoic acid (BA) at a concentration of 20 mmol L^{-1} could capture more than about 99% of $OH^{\bullet}$ produced in solution. *p*-Hydroxybenzoic acid (*p*-HBA) generated from the reaction between BA and $OH^{\bullet}$ could be determined at 255 nm by high-performance liquid chromatography (HPLC, Agilent 1200). The concentration of accumulated $OH^{\bullet}$ was about 5.9 times that of *p*-hydroxybenzoic acid.[29] Therefore, BA (20 mmol L^{-1}) was added to the reaction systems to quantitatively detect the concentration of $OH^{\bullet}$.

3. RESULTS

3.1. Photochemical Formation of Schwertmannite.

The mixed solution of montmorillonite (0.1 g L^{-1}), $NaNO_3$ (100 mmol L^{-1}), and $FeSO_4$ (1.0−5.0 mmol L^{-1}) was exposed to UV light irradiation for 8 h in nitrogen atmosphere at initial pH 6.0. The obtained solid products were determined by XRD. The diffraction peaks at 5.7°, 18.2°, 19.7°, 22.0°, 31.0°, 35.8°, 54.1°, 61.7°, and 73.1° were attributed to montmorillonite (JCPDS No. 02−0014) (Figure 1a).[30] The d_{001} values of montmorillonite, Sch-1Mt, Sch-3Mt, and Sch-5Mt were, respectively, 15.4, 15.9, 16.3, and 17.3 Å, indicating that the interlayer space of the montmorillonite increased with increasing the concentration of $FeSO_4$ in reaction system, which might result from the entry of Fe(II) or Fe(III) into the interlayer of montmorillonite.[31] No obvious diffraction peaks of schwertmannite were observed for Sch-1Mt and Sch-3Mt, possibly due to the low content of schwertmannite on montmorillonite surface, while two newly formed peaks of schwertmannite were observed at 35.2° and 61.3° in the XRD patterns of Sch-5Mt, which corresponded to the (2 1 2) and (0 0 4) planes of schwertmannite, indicating a higher content of schwertmannite in Sch-5Mt than in Sch-1Mt and Sch-3Mt.[32,33] Figure 1b shows the FTIR spectra of montmorillonite and schwertmannite−montmorillonite aggregates. The absorption band at 3628 cm^{-1} is assigned to the Al−OH stretching vibration, and its intensity decreases with increasing $FeSO_4$ concentration.[34] The absorption bands at 3427 and 1633 cm^{-1} are attributed to the O−H stretching and bending vibration in water.[34] The band at 1035 cm^{-1} is assigned to the O−Si−O stretching vibration of montmorillonite. The absorption bands at 919, 792, and 527 cm^{-1} are attributed to the Al−O−H, Al−O, and Al−O−Si bending vibrations, respectively.[34] The absorption band at 705 cm^{-1} was observed for Sch-1Mt, Sch-3Mt, and Sch-5Mt, which corresponds to the Fe−O stretching vibration in schwertmannite.[13] When $FeSO_4$ concentration was increased, the absorption band at 3628 cm^{-1} disappeared, the band at 1035 cm^{-1} shifted to 1028 cm^{-1}, and the intensity of the absorption bands at 909 and 792 cm^{-1} decreased, indicating that M−OH at the edges of the montmorillonite or $M-O^-$ on the montmorillonite surface (M means Al or Si) could form hydrogen bonds and coordination bonds of Si−O···Fe and Al−O···Fe with the ≡Fe−OH of schwertmannite.[32,33]

To investigate the effect of montmorillonite on the photochemical formation of schwertmannite, another photochemical experiment was performed under the similar conditions in the absence of montmorillonite. Figure 1c shows that the diffraction peaks at 18.2°, 26.3°, 35.2°, 39.5°, 46.5°, 55.3°, and 61.3°, respectively, correspond to the (2 1 0), (3 1 0), (2 1 2), (3 0 2), (1 1 3), (5 2 2), and (0 0 4) planes of schwertmannite (JCPDS card No. 47−1775), indicating the formation of single-phase schwertmannite (Sch-1, Sch-3, and Sch-5).[13] The intensity of the major peaks at 35.2° and 61.3° of schwertmannite followed the order of Sch-5 > Sch-3 > Sch-1, indicating that the crystallinity degree of schwertmannite increased with increasing $FeSO_4$ concentration. For single-phase schwertmannite, the bands at 1124, 975, and 610 cm^{-1} are attributed to the S−O stretching vibration in sulfate, and the absorption bands at 700 and 466 cm^{-1} are due to the Fe−O stretching vibrations in schwertmannite (Figure 1d).[35] Schwertmannite would be generated on montmorillonite surface in the form of nanoparticles rather than aggregates, which could increase its specific surface area. The particle size and crystallinity degree of schwertmannite on montmorillonite increased, and urchin-like schwertmannite was gradually formed with increasing concentration of $FeSO_4$. The increase in SO_4^{2-} concentration contributed much to the formation of urchin-like schwertmannite when Fe(II) concentration was kept constant.[13] As a structural component, SO_4^{2-} in high concentration contributed to the formation of coordination bonds between SO_4^{2-} and Fe(II), indicating that SO_4^{2-} played an important role in the formation process of schwertmannite.[10]

In order to further test the possibility of ferrihydrite formation in the photochemical reaction, the samples of Sch-1Mt, Sch-5Mt, and Sch-5 were characterized by Mössbauer spectra measurement. The spectra of Sch-5 showed the characteristic features of schwertmannite in the paramagnetic state (center shifts vs metallic Fe, 0.47 mm s^{-1}, quadrupole splitting, −0.11 mm s^{-1}, and magnetic hyperfine field, 45.9 T) (Figure S1), while the magnetic hyperfine field of ferrihydrites spans the range of 46.5 to 50 T.[36,37] The spectra of Sch-1Mt and Sch-5Mt had no obvious differences from those of single-phase schwertmannite. Taking the above XRD, SEM, and Mössbauer results together, it could be concluded that the iron oxides formed on montmorillonite were schwertmannite.

Figure 2 shows the SEM images of schwertmannite−montmorillonite aggregates and single-phase schwertmannites. Montmorillonite had a flat surface (Figure S2), and fine nanoparticles were formed on the surface when the concentration of $FeSO_4$ was 1.0 mmol L^{-1} (Figure 2a). With $FeSO_4$ concentration increasing to 3.0 mmol L^{-1}, schwertmannite particles were formed and agglomerated on montmorillonite surface (Figure 2b). Urchin-like architectures composed of nanosized fibers were observed on the montmorillonite surface at a higher $FeSO_4$ concentration of 5.0 mmol L^{-1} (Figure 2c), exhibiting a similar morphology to single-phase schwertmannite (Figure 2d−f).[13] The particle size of schwertmannite formed on montmorillonite surface increased with increasing concentration of $FeSO_4$ (Figure 2). These results indicated the formation of schwertmannite on montmorillonite surface during the photochemical process. In order to study the effect of SO_4^{2-} concentration on the micromorphology of the photochemically synthesized schwertmannite, the SO_4^{2-} concentration in the reaction systems was controlled at 5.0 mmol L^{-1} by the addition of Na_2SO_4. Urchin-like schwertmannite was formed (Figure S3) and the intensity of the stretching vibration at 697 cm^{-1} corresponding to Fe−O bonds increased with increasing SO_4^{2-} concentration (Figure S4), indicating that the crystallinity degree of schwertmannite increased with increasing SO_4^{2-} concentration.

DOI: 10.1021/acsearthspacechem.8b00202
ACS Earth Space Chem. 2019, 3, 718−727

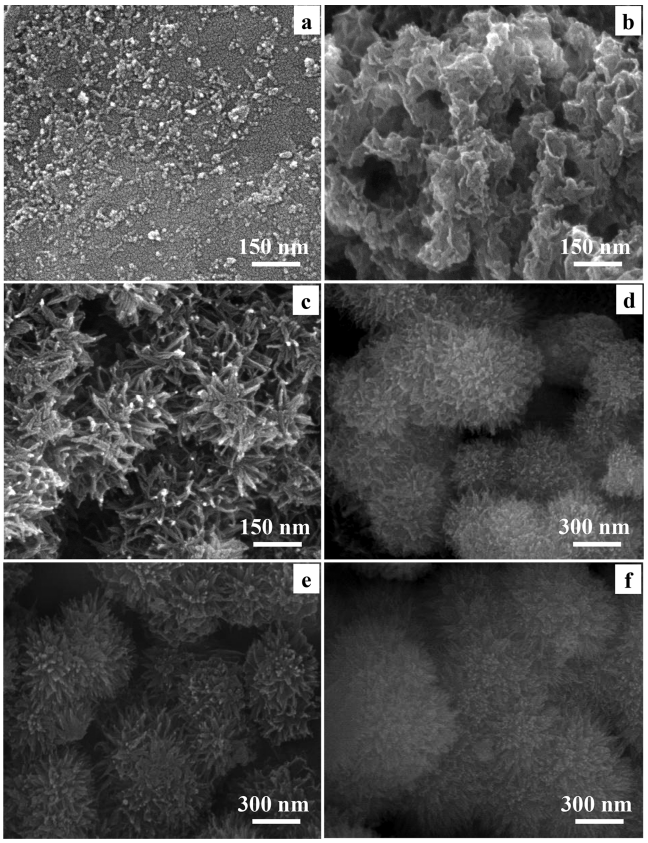

Figure 2. SEM images of Sch-1Mt (a), Sch-3Mt (b), Sch-5Mt (c), Sch-1 (d), Sch-3 (e), and Sch-5 (f).

When $FeSO_4$ concentration was 1.0 mmol L^{-1}, needle-like schwertmannite was observed on the surface and edge of montmorillonite, and some dissociative schwertmannite particles were observed in Figure 3c,d. With increasing concentration of $FeSO_4$ (3.0 and 5.0 mmol L^{-1}), more dissociative schwertmannite particles were observed (Figure 3e–h). The above results indicated that Fe(II) was directly oxidized to schwertmannite or grew on the surface of montmorillonite, and high-concentration $FeSO_4$ contributed to the homogeneous nucleation of schwertmannite.

To identify the role of irradiation in Fe(II) oxidation, the control experiments were conducted under dark. No obvious decrease in the Fe(II) concentrations was observed in 5.0 mmol L^{-1} at pH 6.0 without irradiation, indicating that photochemical process contributes the formation of iron oxides (Figure S5). In order to investigate the possible intermediates of ROS during the photochemical reaction, methanol (100 mmol L^{-1}) and NBT (100 mg L^{-1}) were added to the reaction systems to, respectively, scavenge $OH^{\bullet}$ and $O_2^{\bullet-}$.[13,29] BA (20 mmol L^{-1}) was added to the mixed solution to quantify the $OH^{\bullet}$. Due to the short life span of free radicals, the accurate detection of $O_2^{\bullet-}$ concentration is often conducted under in situ conditions. We did not determine the concentration of $O_2^{\bullet-}$ due to the limitation of experimental conditions. NBT is extremely sensitive to the presence of an electron donor, such as $O_2^{\bullet-}$. Therefore, the reaction between NBT and $O_2^{\bullet-}$ was also carried out to identify the role of $O_2^{\bullet-}$.[38] Figure 4a shows the Fe(II) concentrations in the mixed solution of $NaNO_3$ (100 mmol L^{-1}), $FeSO_4$ (5.0 mmol L^{-1}), montmorillonite (0.1 g L^{-1}), and different scavengers at different time. In the presence of methanol and NBT, the

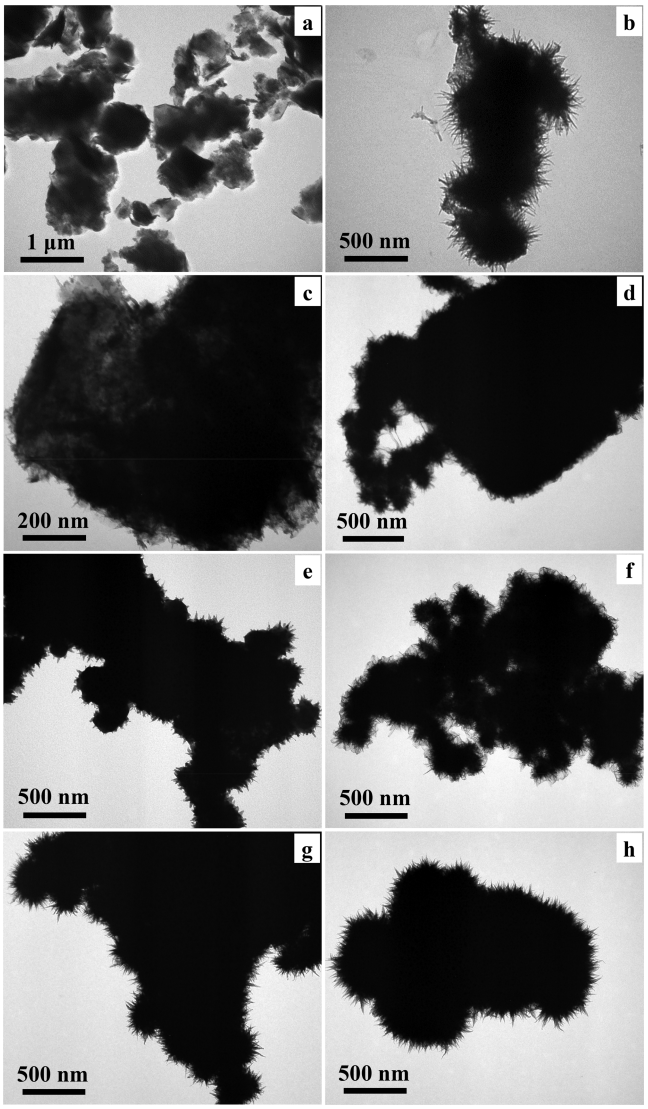

Figure 3. TEM images of montmorillonite (a), Sch-5 (b), Sch-1Mt (c,d), Sch-3Mt (e,f), and Sch-5Mt (g,h).

concentration of oxidized Fe(II) decreased from 2.61 to 1.30 and 0.58 mmol L^{-1}, respectively, indicating a decrease in Fe(II) consumption. The concentration of *p*-HBA was detected to be 0.02 mmol L^{-1} in the presence of BA, suggesting the formation of $OH^{\bullet}$ intermediate (0.12 mmol L^{-1}) in the photochemical process (Figure 4b). These results demonstrated that the $OH^{\bullet}$ and $O_2^{\bullet-}$ generated from the photolysis of NO_3^- are the main oxidants for the photochemical oxidation of Fe(II).

3.2. Cr(VI) Adsorption of Schwertmannite. Figure 5 shows the isotherms of Cr(VI) adsorption on different schwertmannite samples at pH 6.0. The adsorption isotherms were confirmed to be L-type and were well fitted by the Langmuir model. The maximum adsorption capacities of Sch-1, Sch-3, Sch-5, Mt, Sch-1Mt, Sch-3Mt, and Sch-5Mt were 35.8, 38.3, 37.9, 3.2, 19.1, 29.0, and 36.3 mg g^{-1}, respectively (Table 2). The Fe content of Sch-1, Sch-3, Sch-5, Sch-1Mt, Sch-3Mt, and Sch-5Mt was 52.0%, 51.1%, 50.4%, 26.8%, 36.1%, and 38.9%, respectively (Table 2). In order to better represent the adsorption capacity of different schwertmannite samples, the adsorption capacity was normalized to per unit mass of Fe. The adsorption capacity per unit mass of Fe of

DOI: 10.1021/acsearthspacechem.8b00202
ACS Earth Space Chem. 2019, 3, 718–727

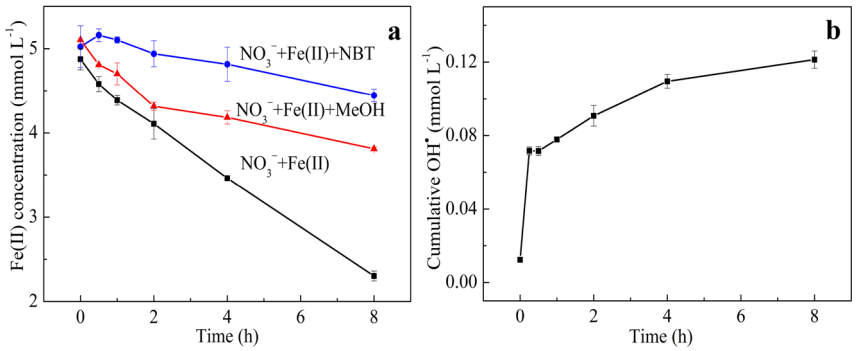

Figure 4. Concentrations of Fe(II) in different reaction systems (a) and $OH^•$ concentration (b) in a mixed solution of $NaNO_3$ (100 mmol L^{-1}), $FeSO_4$ (5.0 mmol L^{-1}), and montmorillonite (0.1 g L^{-1}) with initial pH 6.0 under UV irradiation at different time in nitrogen atmosphere.

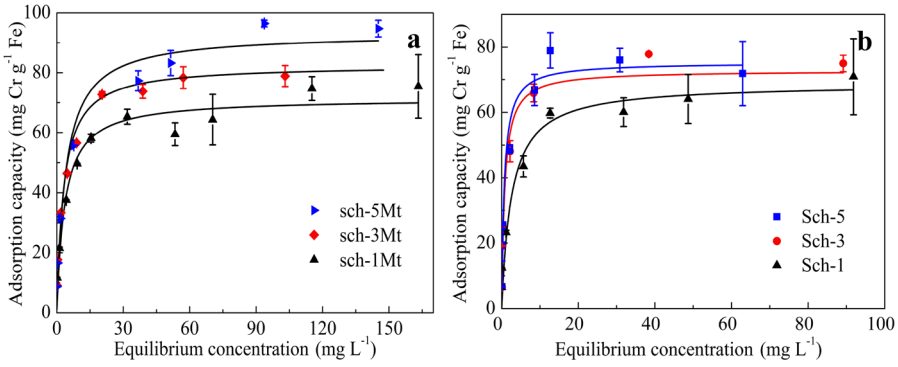

Figure 5. Adsorption isotherms of Cr(VI) on schwertmannite (Sch-1, Sch-3, Sch-5) (a), and montmorillonite (Mt) and schwertmannite–montmorillonite aggregates (Sch-1Mt, Sch-3Mt, Sch-5Mt) (b) with pH 6.0 at 25 °C for 24 h.

Table 2. Total Fe Content of As-obtained Products and Their Cr(VI) Absorption Capacity

sample	Fe (%)	Cr(VI) adsorption capacity (mg g^{-1})	Cr(VI) adsorption capacity per Fe unit mass (mg Cr g^{-1} Fe)	adsorption capacity per specific surface area (μg Cr m^{-2})
Mt	3.4	3.2		23.2
Sch-1	52.0	35.8	68.8	1455.3
Sch-3	51.1	38.3	74.9	1387.7
Sch-5	50.4	37.9	75.2	1533.3
Sch-1Mt	26.8	19.1	71.3	86.0
Sch-3Mt	35.1	29.0	80.3	137.3
Sch-5Mt	38.9	36.3	97.4	160.9

these samples followed the order of Sch-5Mt (97.4 mg Cr g^{-1} Fe) > Sch-3Mt (80.3 mg Cr g^{-1} Fe) > Sch-1Mt (71.3 mg Cr g^{-1} Fe), and Sch-5 (75.2 mg Cr g^{-1} Fe) > Sch-3 (74.9 mg Cr g^{-1} Fe) > Sch-1 (68.8 mg Cr g^{-1} Fe) (Table 2), indicating that the Cr(VI) adsorption of schwertmannite was increased by the formation of montmorillonite–schwertmannite aggregate, and the adsorption capacity per unit mass of Fe gradually increased with increasing $FeSO_4$ concentration in the formation system of schwertmannite.

The Cr(VI) adsorption isotherms of Sch-5Mt at different pH values are shown in Figure S6. Cr(VI) adsorption capacity on schwertmannite increased with decreasing pH. The desorption experiment showed that there was no Cr(III) on the surface of schwertmannite (Figure S7). Mössbauer spectra showed that only Fe(III) was formed in schwertmannite and the aggregates (Figure S1). Cr(III) was not detected in the adsorption experiments as shown in Figure S7. Figure S8 shows no obvious decrease in the concentration of NO_3^- after 24 h of reaction, indicating that schwertmannite had little absorption capacity for NO_3^-.

4. DISCUSSION

4.1. Photochemical Formation Mechanism of Schwertmannite. Schwertmannite is commonly found in acidic-sulfate environments.[1] The formation of schwertmannite from Fe(II) generally involves two processes: the oxidation of Fe(II) to Fe(III) and then complexation with OH^- and SO_4^{2-}.[10] Under acidic conditions, the oxidation of Fe(II) by O_2 is very slow, and the formation of schwertmannite takes a long time (33 d).[10] The natural schwertmannite found in Mitteldeutschland lakes (Lausitz region, Germany) is large nanoparticles with a specific surface area of 72 m^2 g^{-1} and has an urchin-like architecture composed of spherical particles.[10] In this work, the specific surface area of single-phase schwertmannite formed by photochemical formation pathway was 24.6 m^2 g^{-1} (Table S1). Single-phase schwertmannite in the form of aggregate crystals was obtained within 8 h, indicating that sunlight-mediated photochemical processes serve as an important driver for the cycling of Fe in redox environment.

Schwertmannite was synthesized through the photocatalytic oxidation of Fe(II) in NO_3^--containing solution.[13] $NO_2^•$, $O(^3P)$, and $OH^•$ radicals can be generated through the $n \rightarrow \pi^*$ and $\pi \rightarrow \pi^*$ electronic transition processes during the photolysis of NO_3^-.[39,40] In this work, $Fe(II)_{aq}$ could be oxidized to $Fe(III)_{aq}$ by these ROS under anoxic conditions. Our previous work has suggested that $O_2^{•-}$ is the main oxidant

DOI: 10.1021/acsearthspacechem.8b00202
ACS Earth Space Chem. 2019, 3, 718–727

in the photochemical oxidation of Fe(II) and Mn^{2+}.[13,41] When methanol and NBT were added to the suspensions, the oxidation amount of Fe(II) was, respectively, decreased by 50.2% and 77.8%, indicating the generation of $OH^{\bullet}$ and $O_2^{\bullet-}$ in the photochemical reaction, and $O_2^{\bullet-}$ was the main oxidant for the formation of schwertmannite (Figure 4a). Although the quartz tube was sealed by plastic membrane to maintain the anoxic conditions in the photochemical experiments, dissolved oxygen was still detected in the reaction systems (0.3 ppm), which could react with NO_2^- to form $O_2^{\bullet-}$.[41] After the oxidation of Fe(II), the main components of the solution were Fe(III) and SO_4^{2-}. The species and structure of Fe(III) (hydr)oxides depend on the pH value and the anion species of the reaction system.[10] Schwertmannite is widely distributed in acidic and sulfate-rich environments.[2] In this work, the pH of the reaction systems rapidly decreased to an acid range during the photochemical reaction (Figure S9). The low pH would facilitate SO_4^{2-} to compete with OH^- for binding Fe(III) oxides, which would inhibit the formation of single-phase Fe(III) oxides and contribute much to the formation of schwertmannite.[10] The higher concentration of SO_4^{2-} is favorable for the formation of schwertmannite for the binding of Fe with SO_4^{2-}.

In this work, schwertmannite was observed to be uniformly generated on montmorillonite surface (Figure 2a). The PZC values of Fe(III) oxide-clay mineral aggregates were generally lower than those of corresponding single-phase Fe(III) oxides.[18] For example, the PZC value of natural ferrihydrite containing silicate is usually 5.3−7.5, which is lower than that of synthetic ferrihydrite (pH_{PZC} 8.0).[18] In this work, the PZC value of montmorillonite−schwertmannite aggregates was higher than that of single montmorillonite (pH_{PZC} 2.75), and lower than that of single schwertmannite sample (pH_{PZC} 6.24) (Figure 6), suggesting that the net point of zero charges of the

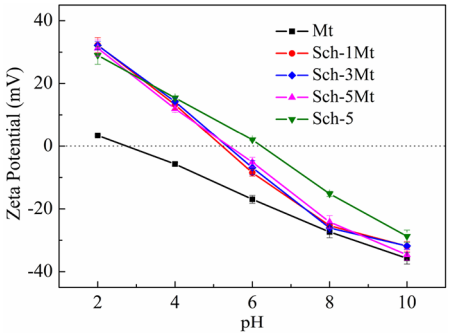

Figure 6. Zeta potential of montmorillonite (Mt), Sch-1Mt, Sch-3Mt, Sch-5Mt, and Sch-5 (1.5 g L^{-1}) at different pHs in 1.0 mmol L^{-1} $NaNO_3$ solution.

aggregates decreased in the presence of montmorillonite. The final pH values sharply decreased to be below 3.0 in the reaction systems of photochemical formation of schwertmannite (Figure S9). Under the low pH conditions, the basal surface of the montmorillonite was negatively charged and schwertmannite was positively charged (Figure 6). Therefore, the aggregation of montmorillonite particles and schwertmannite particles was easily driven by electrostatic force.

Montmorillonite affects the physicochemical properties including the morphology and particle size of schwertmannite, suggesting heterogeneous nucleation mechanism. Montmorillonite can adsorb $Fe(II)_{aq}$ owing to its net negative surface charge. The maximum Fe(II) adsorption capacity of montmorillonite is 10.93 mg L^{-1} at pH 6.0 (Figure S10). $Fe(II)_{ads}$ on montmorillonite surface can be oxidized to Fe(III) by ROS generated from the photolysis of NO_3^-. The negative electric field of the clay can accelerate the hydrolysis of Fe(III), leading to the formation of schwertmannite on montmorillonite surface.[42,43] Single-phase schwertmannite is composed of spherical particles with a larger particle size and a regular morphology in the absence of montmorillonite (Figure 2). Compared with single-phase schwertmannite, the schwertmannite formed on the montmorillonite surface is composed of fine nanoparticles (Figure 2). The presence of montmorillonite could prevent the intense aggregation of schwertmannite particles due to the larger surface area of montmorillonite; therefore, more schwertmannite particles could be nucleated and grew on the surface of montmorillonite.[10] The rapid heteroaggregation of freshly formed schwertmannite with montmorillonite could prevent the further growth of schwertmannite crystal. Therefore, the freshly formed schwertmannite existed as small and irregular spherical particles on the surface of montmorillonite.

4.2. Effect of Montmorillonite on Cr(VI) Adsorption of Schwertmannite. The Cr(VI) absorption capacity of single-phase schwertmannite samples (Sch-1, Sch-3, and Sch-5) shows no obvious differences because of their similarities in porous structure, specific surface area, and morphology (Figure 2 and Table S1); while there are obvious increases in the maximum adsorption capacity of Sch-1Mt, Sch-3Mt, and Sch-5Mt depending on $FeSO_4$ concentration (Table 2). In general, the specific surface area and porous volume of schwertmannite increase with increasing $FeSO_4$ concentration in the reaction system.

Montmorillonite has a specific surface area as large as 138 m^2 g^{-1} and shows a low Cr(VI) adsorption capacity (3.2 mg g^{-1}) (Table 2). Schwertmannite plays a more important role than montmorillonite in the Cr(VI) adsorption process. The large specific surface area and high PZC of schwertmannite facilitate the adsorption of Cr(VI).[3] Previous studies have indicated that the large specific surface area and pore volume contribute much to the arsenate adsorption capacity of schwertmannite.[44] The coaggregation of nanoparticles often decreases the effective surface area of nanoparticles and reduces their reaction activities.[30] The size of hysteresis loop in the montmorillonite−schwertmannite aggregates follows the order of Sch-1Mt > Sch-3Mt > Sch-5Mt (Figure S11), suggesting that the entry of Fe(II) or Fe(III) into the interlayer of montmorillonite.[30,31] The insertion into montmorillonite increases the specific surface area and the porous volume of aggregates, which elevates the corresponding Cr(VI) adsorption capacity. The adsorption capacity of Sch-1Mt, Sch-3Mt, and Sch-5Mt is 71.3, 80.3, and 97.4 mg Cr g^{-1} Fe, respectively. As for SchMt-1, SchMt-3, and SchMt-5, the Fe percentages of the products, respectively, reach 26.8%, 36.1%, and 38.9%, accompanied by an increase in Cr(VI) adsorption capacity per unit mass of Fe.

The Cr adsorption capacity is determined not only by the specific surface area but also by the amount of adsorption site in absorbents. Although the specific surface area of Sch-1Mt (222.1 m^2 g^{-1}) is much larger than that of Sch-1 (24.6 m^2 g^{-1}), the Cr adsorption capacity per unit mass of Fe of Sch-1Mt is not significantly higher than that of Sch-1. Although montmorillonite has a large specific surface area, it has very low adsorption capacity for Cr(VI). The Cr(VI) adsorption

DOI: 10.1021/acsearthspacechem.8b00202
ACS Earth Space Chem. 2019, 3, 718−727

capacity per specific surface area of single-phase schwertmannite is much higher than that of schwertmannite−montmorillonite aggregates likely due to the complexation of Cr(VI) and hydroxyl.[3] The coordination chemistry of iron affects the adsorption capacity of corresponding Fe(III) oxides for anions.[10] Clay minerals (silicate) are considered to compete with OH^- for binding Fe(III) oxides during the formation process.[10,15,16] During the formation process of schwertmannite−montmorillonite aggregates, montmorillonite could bind with the hydroxyl groups of schwertmannite, which would decrease the active sites for Cr(VI) adsorption. However, the Cr adsorption capacity per unit mass of Fe of Sch-1Mt is not significantly higher than that of Sch-1, possibly due to the exposure of more active adsorption sites for the complexation reaction of schwertmannite on montmorillonite surface under UV irradiation. When the initial concentration of montmorillonite was controlled at a constant level, epitaxial growth would occur on the surface of newly formed schwertmannite due to the limited number of complexation sites of montmorillonite with increasing $FeSO_4$ concentration. The complexation of schwertmannite with montmorillonite decreases with increasing $FeSO_4$ concentration of reaction system. The Cr(VI) adsorption capacity per unit mass of Fe in minerals increases with increasing Fe concentration, resulting in the highest Cr(VI) adsorption capacity of Sch-5Mt, likely due to the increase in porous structure and corresponding adsorption sites (hydroxyl groups), which could contribute to the coordination with Cr(VI) on schwertmannite surface.

5. ENVIRONMENTAL SIGNIFICANCE

The development of industrial civilization has caused many environmental problems including the pollution of waters and soils.[41] Due to their larger specific surface areas and surface active sites, iron oxides are important sinks for heavy metal ions in soils and sediments. Therefore, the formation and transformation of iron oxides significantly affect the adsorption, redox, and migration behavior of metal cations (such as Al^{3+}, Mn^{2+}, Cu^{2+}, Zn^{2+}, Co^{2+}, Ni^{2+}, and Pb^{2+}) and anions (such as AsO_4^{3-}, CrO_4^{2-}, and MoO_4^{2-}) in natural environments.[13] The photochemical reactions initiated by sunlight irradiation are ubiquitous in natural environments. For example, the speciation and concentration of heavy metal ions in surface waters of alpine streams are associated with the diel periodic changes in the photochemical reactions of iron oxides.[45] However, little is known about the influence of light irradiation on the formation of iron oxides from the oxidation of Fe^{2+} and the subsequent adsorption for heavy metal ions.

Light can penetrate into soil and mineral particles with a thickness of about 5−6 mm and reach about 100 m depth underwater through a water column.[14] Many substances including dissolved NO_3^- and NO_2^- were found to be photoreactive, and they can generate reactive oxygen species in natural aqueous systems.[41] In our previous work, we have found that schwertmannite could be formed for the photocatalytic oxidation of Fe^{2+} in the presence of low concentration NO_3^- (0.2 mmol L^{-1}).[13] The oxidation of Fe^{2+} to schwertmannite may occur slowly with a low concentration of NO_3^- under natural conditions.[13] In this work, the concentrations of NO_3^- and Fe^{2+} were, respectively, controlled at 100 and 1.0−5.0 mmol L^{-1}. These concentrations of Fe^{2+} can be commonly found on some sediment−water interfaces under anoxic conditions.[46] The present work shows that the schwertmannite−montmorillonite aggregate could be generated through the oxidation of Fe^{2+} on montmorillonite by reactive oxygen species under UV irradiation, indicating the possible formation processes of iron oxides in natural environments.

The complex chemical composition comprising organic matters, clay minerals, and heavy metal ions has been reported in the natural soil system.[14] Besides the possible photochemical reactions as mentioned above, many other substances may also participate in the photochemical mineralization of various iron oxides and the corresponding complexes. The generation of iron oxides could influence the adsorption−desorption and redox of heavy metal ions. This work just shows the possible photochemical formation processes of schwertmannite on montmorillonite and the corresponding Cr(VI) adsorption capacity, which contributes to a better understanding of the potential photochemical mineralization process of iron oxides and environmental chemistry behavior, although the photochemical formation processes need to be further studied in complex environments.

6. CONCLUSIONS

Schwertmannite was photochemically generated on montmorillonite surface due to the oxidation of $Fe(II)_{ads}$ by $O_2^{\bullet-}$ and $OH^{\bullet}$ generated from the photolysis of NO_3^-. The presence of montmorillonite decreased the growth and aggregation of schwertmannite crystal particles as well as the crystallinity degree of schwertmannite. The schwertmannite was coated on the surface of montmorillonite and increased with increasing concentration of Fe(II) in the reaction system, which increased the available adsorption sites of schwertmannite and improved its Cr(VI) adsorption capacity. Due to the dispersing effect of montmorillonite on the photochemical formation process of schwertmannite, the specific surface area of schwertmannite increased from 24.6 to 243.3 $m^2\ g^{-1}$, and correspondingly, the Cr(VI) adsorption capacity increased from 71.3 to 97.4 mg Cr g^{-1} Fe. The present work indicates that the formation of schwertmannite on clay mineral montmorillonite facilitates a high absorption capacity for Cr(VI).

■ ASSOCIATED CONTENT

Supporting Information

The Supporting Information is available free of charge on the ACS Publications website at DOI: 10.1021/acsearthspacechem.8b00202.

Porous structural data of the samples; Mössbauer spectra of Sch-1Mt, Sch-5Mt, and Sch-5; FESEM images of montmorillonite; FESEM images and FTIR spectra of Sch-1Mt, Sch-1Mt-4S, Sch-3Mt, and Sch-3Mt-2S; XRD patterns of final products and the changes of Fe(II) concentrations under dark conditions; Cr(VI) adsorption on Sch-5Mt at different pH values; Cr desorption on Sch-5Mt; Changes of NO_3^- concentration; Changes of pH; Adsorption isotherms of Fe(II) on the montmorillonite; Nitrogen adsorption−desorption isotherms of Sch-1, Sch-3, Sch-5, Sch-1Mt, Sch-3Mt, and Sch-5Mt (PDF)

■ AUTHOR INFORMATION

Corresponding Author

*E-mail: qiugh@mail.hzau.edu.cn.

DOI: 10.1021/acsearthspacechem.8b00202
ACS Earth Space Chem. 2019, 3, 718−727

ORCID

Guohong Qiu: 0000-0002-1181-3707
Wenfeng Tan: 0000-0002-3098-2928
Chengshuai Liu: 0000-0003-0133-0119

Notes

The authors declare no competing financial interest.

■ ACKNOWLEDGMENTS

This work was supported by the National Natural Science Foundation of China (Grant Nos. 41571228, 41877025, and 41425006), the National Key Research and Development Program of China (Grant Nos. 2018YFD0800304 and 2017YFD0801000), and the Fundamental Research Funds for the Central Universities (Nos. 2662018JC055 and 2662015JQ002) for financial support. The authors thank Dr. Lihong Qin and Dr. Jianbo Cao at the Public Laboratory of Electron Microscopy of Huazhong Agricultural University for the help in FESEM characterization.

■ REFERENCES

(1) Bigham, J. M.; Schwertmann, U.; Traina, S. J.; Winland, R. L.; Wolf, M. Schwertmannite and the chemical modeling of iron in acid sulfate waters. *Geochim. Cosmochim. Acta* **1996**, *60*, 2111−2121.

(2) Wang, X. M.; Gu, C.; Feng, X. H.; Zhu, M. Q. Sulfate local coordination environment in schwertmannite. *Environ. Sci. Technol.* **2015**, *49*, 10440−10448.

(3) Antelo, J.; Fiol, S.; Gondar, D.; Lopez, R.; Arce, F. Comparison of arsenate, chromate and molybdate binding on schwertmannite: surface adsorption vs anion-exchange. *J. Colloid Interface Sci.* **2012**, *386*, 338−343.

(4) Zhang, Y. C.; Li, J.; Zhang, M.; Dionysiou, D. D. Size-tunable hydrothermal synthesis of SnS_2 nanocrystals with high performance in visible light-driven photocatalytic reduction of aqueous Cr(VI). *Environ. Sci. Technol.* **2011**, *45*, 9324−9331.

(5) Regenspurg, S.; Peiffer, S. Arsenate and chromate incorporation in schwertmannite. *Appl. Geochem.* **2005**, *20*, 1226−1239.

(6) Burton, E. D.; Johnston, S. G.; Kraal, P.; Bush, R. T.; Claff, S. Sulfate availability drives divergent evolution of arsenic speciation during microbially mediated reductive transformation of schwertmannite. *Environ. Sci. Technol.* **2013**, *47*, 2221−2229.

(7) Xiong, H. X.; Liao, Y. H.; Zhou, L. X. Influence of chloride and sulfate on formation of akaganéite and schwertmannite through ferrous biooxidation by acidithiobacillus ferrooxidans cells. *Environ. Sci. Technol.* **2008**, *42*, 8681−8686.

(8) Liu, F. W.; Zhou, J.; Zhang, S. S.; Liu, L. L.; Zhou, L. X.; Fan, W. H. Schwertmannite synthesis through ferrous ion chemical oxidation under different H_2O_2 supply rates and its removal efficiency for Arsenic from contaminated groundwater. *PLoS One* **2015**, *10*, 1−14.

(9) Murad, E.; Rojík, P. Jarosite, schwertmannite, goethite, ferrihydrite and lepidocrocite: The legacy of coal and sulfide ore mining. In *3rd Australian New Zealand Soils Conference*, University of Sydney Australia, 2004.

(10) Regenspurg, S.; Brand, A.; Peiffer, S. Formation and stability of schwertmannite in acidic mining lakes. *Geochim. Cosmochim. Acta* **2004**, *68*, 1185−1197.

(11) Eskandarpour, A.; Onyango, M. S.; Tanahashi, M.; Ochieng, A.; Bando, Y.; Iwai, K.; Okido, M.; Asai, S. Magnetic fixed-bed column for Cr(VI) removal from aqueous solution using schwertmannite. *ISIJ Int.* **2008**, *48*, 240−244.

(12) Chen, F. X.; Zhou, L. X. Adsorption of Cr(VI) in wastewater by catalytic biosynthesis Schwertmannite. *Chin. Environ. Sci.* **2006**, *26*, 11−15.

(13) Liu, L. H.; Jia, Z. H.; Tan, W. F.; Suib, S. L.; Ge, L.; Qiu, G. H. Abiotic photomineralization and transformation of iron oxide nanominerals in aqueous systems. *Environ. Sci.: Nano* **2018**, *5*, 1169−1178.

(14) Melton, E. D.; Swanner, E. D.; Behrens, S.; Schmidt, C.; Kappler, A. The interplay of microbially mediated and abiotic reactions in the biogeochemical Fe cycle. *Nat. Rev. Microbiol.* **2014**, *12*, 797−808.

(15) Kaegi, R.; Voegelin, A.; Folini, D.; Hug, S. J. Effect of phosphate, silicate, and Ca on the morphology, structure and elemental composition of Fe(III)-precipitates formed in aerated Fe(II) and As(III) containing water. *Geochim. Cosmochim. Acta* **2010**, *74*, 5798−5816.

(16) Jones, A. M.; Collins, R. N.; Rose, J.; Waite, T. D. The effect of silica and natural organic matter on the Fe(II)-catalysed transformation and reactivity of Fe(III) minerals. *Geochim. Cosmochim. Acta* **2009**, *73*, 4409−4422.

(17) Wang, X. M.; Zhu, M. Q.; Lan, S.; Ginder-Vogel, M.; Liu, F.; Feng, X. H. Formation and secondary mineralization of ferrihydrite in the presence of silicate and Mn(II). *Chem. Geol.* **2015**, *415*, 37−46.

(18) Schwertmann, U.; Taylor, R. M. *Iron Oxides*; Soil Science Society of America: Madison, WI, 1989.

(19) Zarzycki, P.; Szabelski, P.; Piasecki, W. Modelling of ζ-potential of the montmorillonite/electrolyte solution interface. *Appl. Surf. Sci.* **2007**, *253*, 5791−5796.

(20) Chakraborty, S.; Favre, F.; Banerjee, D.; Scheinost, A. C.; Mullet, M.; Ehrhardt, J. J.; Brendle, J.; Vidal, L.; Charlet, L. U(VI) sorption and reduction by Fe(II) sorbed on montmorillonite. *Environ. Sci. Technol.* **2010**, *44*, 3779−3785.

(21) Soltermann, D.; Fernandes, M. M.; Baeyens, B.; Dahn, R.; Miehe-Brendle, J.; Wehrli, B.; Bradbury, M. H. Fe(II) sorption on a synthetic montmorillonite. A combined macroscopic and spectroscopic study. *Environ. Sci. Technol.* **2013**, *47*, 6978−6986.

(22) Soltermann, D.; Fernandes, M. M.; Baeyens, B.; Dahn, R.; Joshi, P. A.; Scheinost, A. C.; Gorski, C. A. Fe(II) uptake on natural montmorillonites. I. Macroscopic and spectroscopic characterization. *Environ. Sci. Technol.* **2014**, *48*, 8688−8697.

(23) Hou, T.; Xu, R.; Tiwari, D.; Zhao, A. Interaction between electrical double layers of soil colloids and Fe/Al oxides in suspensions. *J. Colloid Interface Sci.* **2007**, *310*, 670−674.

(24) Hou, T.; Xu, R.; Zhao, A. Interaction between electric double layers of kaolinite and Fe/Al oxides in suspensions. *Colloids Surf., A* **2007**, *297*, 91−94.

(25) Wei, S. Y.; Tan, W. F.; Liu, F.; Zhao, W.; Weng, L. P. Surface properties and phosphate adsorption of binary systems containing goethite and kaolinite. *Geoderma* **2014**, *213*, 478−484.

(26) Collins, R. N.; Jones, A. M.; Waite, T. D. Schwertmannite stability in acidified coastal environments. *Geochim. Cosmochim. Acta* **2010**, *74*, 482−496.

(27) Tamura, H.; Goto, K.; Yotsuyanagi, T.; Nagayama, M. Spectrophotometric determination of iron(II) with 1,10-phenanthroline in the presence of large amounts of iron(III). *Talanta* **1974**, *21*, 314−318.

(28) Rand, M. S.; Greenberg, A. E.; Taras, M. J. Standard methods for the examination of water and wastewater. *Inter. J. Env. Res. Pub.* **1975**, *56*, 387−388.

(29) Hong, J.; Liu, L. H.; Luo, Y.; Tan, W. F.; Qiu, G. H.; Liu, F. Photochemical oxidation and dissolution of arsenopyrite in acidic solutions. *Geochim. Cosmochim. Acta* **2018**, *239*, 173−185.

(30) Yuan, P.; Fan, M.; Yang, D.; He, H.; Liu, D.; Yuan, A.; Zhu, J.; Chen, T. Montmorillonite-supported magnetite nanoparticles for the removal of hexavalent chromium [Cr(VI)] from aqueous solutions. *J. Hazard. Mater.* **2009**, *166*, 821−829.

(31) Gao, Y.; Wang, Y.; Zhang, H. Removal of Rhodamine B with Fe-supported bentonite as heterogeneous photo-Fenton catalyst under visible irradiation. *Appl. Catal., B* **2015**, *178*, 29−36.

(32) Ioannou, A.; Dimirkou, A. Phosphate adsorption on hematite, kaolinite, and kaolinite-hematite (k-h) systems as described by a constant capacitance model. *J. Colloid Interface Sci.* **1997**, *192*, 119−128.

(33) Dimirkou, A.; Ioannou, A.; Doula, M. Preparation, characterization and sorption properties for phosphates of hematite, bentonite

DOI: 10.1021/acsearthspacechem.8b00202
ACS Earth Space Chem. 2019, 3, 718−727

and bentonite-hematite systems. *Adv. Colloid Interface Sci.* **2002**, *97*, 37−61.
(34) Bekci, Z.; Seki, Y.; Kadir Yurdakoç, M. A study of equilibrium and FTIR, SEM/EDS analysis of trimethoprim adsorption onto K10. *J. Mol. Struct.* **2007**, *827*, 67−74.
(35) Boily, J. F.; Gassman, P. L.; Peretyazhko, T.; Szanyi, J.; Zachara, J. M. FTIR spectral components of schwertmannite. *Environ. Sci. Technol.* **2010**, *44*, 1185−1190.
(36) Carlson, L.; Bigham, J. M.; Schwertmann, U.; Kyek, A.; Wagner, F. Scavenging of As from Acid Mine Drainage by Schwertmannite and Ferrihydrite: A Comparison with Synthetic Analogues. *Environ. Sci. Technol.* **2002**, *36*, 1712−1719.
(37) Bishop, J. L.; Pieters, C. M.; Burns, R. G. Reflectance spectroscopy of ferric sulfate-bearing montmorillonites as Mars soil analog materials. *Icarus* **1995**, *117*, 101−119.
(38) Hayyan, M.; Hashim, M. A.; AlNashef, I. M. Superoxide Ion: Generation and Chemical Implications. *Chem. Rev.* **2016**, *116*, 3029−3085.
(39) Mack, J.; Bolton, J. R. Photochemistry of nitrite and nitrate in aqueous solution: a review. *J. Photochem. Photobiol., A* **1999**, *128*, 1−13.
(40) Goldstein, S.; Rabani, J. Mechanism of nitrite formation by nitrate photolysis in aqueous solutions: The role of peroxynitrite, nitrogen dioxide, and hydroxyl radical. *J. Am. Chem. Soc.* **2007**, *129*, 10597−10601.
(41) Zhang, T. F.; Liu, L. H.; Tan, W. F.; Suib, S. L.; Qiu, G. H.; Liu, F. Photochemical formation and transformation of birnessite: Effects of cations on micromorphology and crystal structure. *Environ. Sci. Technol.* **2018**, *52*, 6864−6871.
(42) Villalba, J. C.; Constantino, V. R.; Anaissi, F. J. Iron oxyhydroxide nanostructured in montmorillonite clays: Preparation and characterization. *J. Colloid Interface Sci.* **2010**, *349*, 49−55.
(43) Banfield, J. F.; Welch, S. A.; Zhang, H.; Ebert, T. T.; Penn, R. L. Aggregation-based crystal growth and microstructure development in natural iron oxyhydroxide biomineralization products. *Science* **2000**, *289*, 751−754.
(44) Dou, X.; Mohan, D.; Pittman, C. U. Arsenate adsorption on three types of granular schwertmannite. *Water Res.* **2013**, *47*, 2938−2948.
(45) Nimick, D. A.; Gammons, C. H.; Cleasby, T. E.; Madison, J. P.; Skaar, D.; Brick, C. M. Diel cycles in dissolved metal concentrations in streams: occurrence and possible causes. *Water Resour. Res.* **2003**, *39*, 1247.
(46) Lam, B. R.; Rowe, A. R.; Nealson, K. H. Variation in electrode redox potential selects for different microorganisms under cathodic current flow from electrodes in marine sediments. *Environ. Microbiol.* **2018**, *20*, 2270−2287.

DOI: 10.1021/acsearthspacechem.8b00202
ACS Earth Space Chem. 2019, 3, 718−727